Materials Today Bio 27 (2024) 101130

Contents lists available at ScienceDirect

Materials Today Bio

journal homepage: www.journals.elsevier.com/materials-today-bio

Polydopamine-coated bioactive glass for immunomodulation and odontogenesis in pulpitis

Jingyi Li [a,1], Jilin Wu [a,1], Lin Zhu [a], Sicong Mao [b], Sainan Wang [a], Peipei Jia [a], Yanmei Dong [a,*]

[a] Department of Cariology and Endodontology, Peking University School and Hospital of Stomatology & National Clinical Research Center for Oral Diseases & National Engineering Laboratory for Digital and Material Technology of Stomatology & Beijing Key Laboratory of Digital Stomatology, 22 Zhongguancun South Avenue, Haidian District, Beijing, 100081, China

[b] Department of General Dentistry, Peking University School and Hospital of Stomatology & National Clinical Research Center for Oral Diseases & National Engineering Laboratory for Digital and Material Technology of Stomatology & Beijing Key Laboratory of Digital Stomatology, Beijing, 100081, China

ARTICLE INFO

Keywords:
Biomaterials
Polydopamine
Macrophages
Dental pulp capping
Dental pulp disease
Odontogenesis

ABSTRACT

Preserving vital pulp in cases of dental pulpitis is desired but remains challenging. Previous research has shown that bioactive glass (BG) possesses notable capabilities for odontogenic differentiation. However, the immunoregulatory potential of BG for inflamed pulp is still controversial, which is essential for preserving vital pulp in the context of pulpitis. This study introduces a novel approach utilizing polydopamine-coated BG (BG-PDA) which demonstrates the ability to alleviate inflammation and promote odontogenesis for vital pulp therapy. *In vitro*, BG-PDA has the potential to induce M2 polarization of macrophages, resulting in decreased intracellular reactive oxygen species levels, inhibition of pro-inflammatory factor, and enhancement of anti-inflammatory factor expression. Furthermore, BG-PDA can strengthen the mitochondrial function in macrophages and facilitate odontogenic differentiation of human dental pulp cells. In a rat model of pulpitis, BG-PDA exhibits the capacity to promote M2 polarization of macrophages, alleviate inflammation, and facilitate dentin bridge formation. This study highlights the notable immunomodulatory and odontogenesis-inducing properties of BG-PDA for treating dental pulpitis, as evidenced by both *in vitro* and *in vivo* experiments. These results imply that BG-PDA could serve as a promising biomaterial for vital pulp therapy.

1. Introduction

The dental pulp plays a pivotal role in maintaining the structural and functional integrity of the tooth. The development of dental caries and trauma results in irreversible pulp inflammation. Currently, root canal therapy stands as the primary treatment modality for pulpitis, which requires a thorough pulp extirpation to salvage the tooth. Although this procedure effectively relieves symptoms and preserves the affected tooth, the removal of vital pulp tissue compromises the defensive capabilities and sensory functions of the tooth. In recent years, vital pulp therapy (VPT) has emerged as a promising alternative, aiming to preserve the pulp by employing suitable capping materials in areas of pulp exposure. However, conventional materials used for pulp capping in VPT often result in the formation of scar-like tissue or persistent chronic inflammation, leading to unsatisfactory outcomes [1]. Consequently, there is an urgent imperative to develop novel materials capable of effectively modulating the inflammation and facilitating the odontogenesis of inflamed pulp tissue

Reactive oxygen species (ROS) have been found to significantly influence the prognosis of inflammatory diseases, by regulating the expression of inflammatory genes and determining the polarization of macrophage phenotypes [2]. Previous studies have demonstrated that mitochondria within an inflammatory microenvironment consistently generate ROS, leading to compromised mitochondrial function and subsequent tissue damage [3]. Thus, the regulation of mitochondrial metabolism is essential for maintaining macrophage functionality [4,5], which ultimately influences the progress of tissue repair. Polydopamine (PDA)-based materials have garnered considerable attention for their remarkable antioxidant properties and their potential to modulate inflammation effectively [6]. Notably, PDA nanoparticles have demonstrated efficacy in suppressing ROS generation and pro-inflammatory cytokine production, thereby facilitating wound healing and tissue

* Corresponding author.
E-mail address: kqdongyanmei@bjmu.edu.cn (Y. Dong).
[1] These authors contributed equally to this work.

https://doi.org/10.1016/j.mtbio.2024.101130
Received 13 April 2024; Received in revised form 7 June 2024; Accepted 16 June 2024
Available online 21 June 2024

regeneration [7,8]. Furthermore, it has been observed that the degradation byproducts of PDA reduce inflammation in macrophages stimulated by lipopolysaccharide (LPS) [9]. Thus, PDA shows promise as a potential capping material to alleviate inflammation in inflamed pulp for VPT.

In addition to superior anti-inflammatory capacity, the ideal capping material for VPT should also demonstrate the ability to induce mineralization, thereby facilitating the rapid formation of dentin bridge to protect the remaining pulp tissue. Bioactive glass (BG) is a degradable silica-calcium material, known for its excellent bioactivity and mineralization-inducing ability [10]. Our previous study has confirmed that BG demonstrates a significant capacity to stimulate odontogenic differentiation of human dental pulp cells (hDPCs), resulting in dentin bridge formation in a rat pulp-capping model devoid an inflammatory microenvironment [11,12]. Moreover, our research has substantiated that BG retains its exceptional ability to enhance odontogenesis even in an inflammatory microenvironment induced by LPS [13]. However, the immunoregulatory capability of BG for dental pulpitis is still controversial. Previous research has demonstrated that the immunoregulatory capacity of BG is constrained by its composition and the surrounding tissue microenvironment in which they are utilized [14]. Furthermore, the incorporation of functional groups can also impact the mineralization capability of BG [15]. Inspired by mussel adhesive proteins, PDA coating has emerged as a straightforward, effective, and extensional strategy to endow substrate materials with the ability to scavenge extracellular ROS [16] and regulate the macrophage polarization [17]. Moreover, previous research has indicated that PDA exhibits beneficial property in promoting mineralization and that PDA coatings can improve tissue repair [18]. We hypothesize that PDA-coated BG holds promise in alleviating pulp inflammation and facilitating odontogenesis, thereby preserving pulp vitality and safeguarding against reinfection.

This study introduces a novel approach utilizing PDA-coated BG (BG-PDA) for VPT in inflamed pulp. BG-PDA was synthesized via the alkaline-induced self-polymerization of dopamine onto the surface of phytic acid-derived BG. The developed BG-PDA inherited remarkable immunoregulatory ability of PDA while maintaining the odontogenic-inducing ability of BG. This unique combination proved advantageous in facilitating dentin repair of inflamed pulp tissues, thereby contributing to their long-term health and vitality. *In vitro* results showed that BG-PDA can induce the polarization of inflammatory macrophages towards the M2 phenotype by enhancing mitochondrial function. In addition, BG-PDA demonstrated enhanced anti-inflammatory properties and facilitated dentin repair in a rat model of pulpitis. These findings underscore the therapeutic potential of BG-PDA as a promising intervention for repairing inflamed pulp and provide novel insights into the utilization of immunoregulatory materials in treating pulpitis (see Scheme 1).

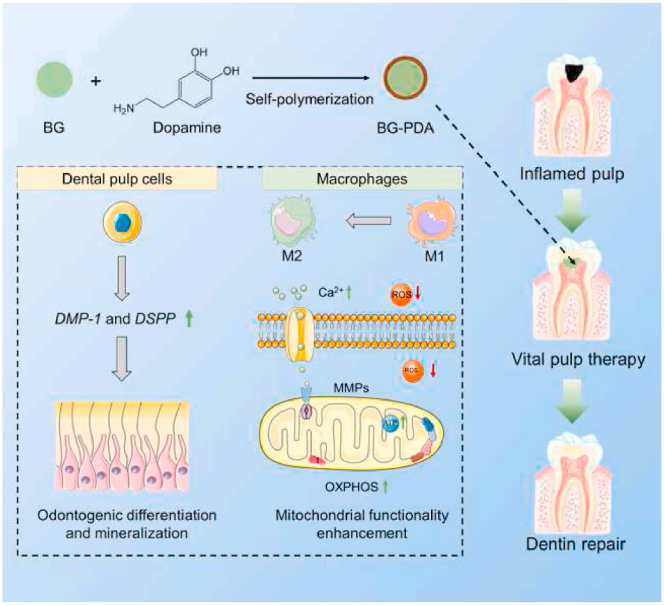

Scheme 1. Schematic illustration of the preparation process of BG-PDA and its application in the vital pulp therapy of inflamed dental pulp. BG-PDA can induce the polarization of inflammatory macrophages towards the M2 phenotype by enhancing mitochondrial function and promote dentin repair by odontogenic-inducing ability.

2. Materials and methods

2.1. Materials

Tris-HCl, dopamine, LPS, Phorbol 12-myristate 13-acetate (PMA), the 3-(4,5-dimethyl-2-thiazolyl)-2,5-diphenyl tetrazolium bromide (MTT) and secondary antibodies were purchased from Sigma-Aldrich (USA). THP-1 cells and fetal bovine serum (FBS) were purchased from Procell Life Science Technology Co., Ltd. (Procell, Wuhan, China). RPMI 1640 medium, Dulbecco's modified Eagle's medium (DMEM) medium, penicillin and streptomycin were purchased from Gibco (MA, USA). CD86 polyclonal and CD206 monoclonal antibodies were purchased from Proteintech (Wuhan, China). Fluor-conjugated secondary antibodies were purchased from Sigma-Aldrich (USA). Secondary antibodies included anti-mouse IgG and anti-rabbit IgG were purchased from Proteintech (Wuhan, China). Enzyme-linked immunosorbent assay (ELISA) was purchased from Thermo Fisher Scientific (MA, USA). Dihydroethidium (DHE) was purchased from Beyotime Biotechnology (Beijing, China). JC-1 mitochondrial membrane potential (MMP) Assay Kit and HE staining was purchased from Solarbio (Beijing, China). XF24 Seahorse was purchased from Agilent Technologies (CA, USA). Ultrasonic working tip (ED15) was purchased from DTE (Beijing, China). The self-adhesive resin was purchased from Kerr (America).

2.2. Synthesis and characterization of BG-PDA

In our previous study, a pH-neutral BG was prepared through the sol-gel method with a nominal molar composition of the BG consisting of 54.2 % SiO_2, 35.0 % CaO, and 10.8 % P_2O_5 [19]. The BG particles were sifted through a 200-mesh sieve to obtain fine particles with an average sized of $\leq$38 μm. BG (4 mg/mL) particles were added into Tris-buffer (10 mM, pH = 8.5), and magnetically stirred to homogenize, and then dopamine (2 mg/mL) was added. The reaction was violently stirred at room temperature away from light, BG-PDA particles were separated via centrifugation at 5000 rpm, washed in deionized water, and subsequently dried. PDA nanoparticles were prepared by self-polymerization of dopamine in Tris-buffer and separated via centrifugation at 10000 rpm, washed in deionized water, and subsequently dried.

The micromorphology of BG-PDA was characterized by scanning electron microscopy (SEM, SU8010, Hitachi). The morphology and integrity of the PDA coating on BG was investigated by transmission electron microscopy (TEM, JEM1011, Jeol). The energy dispersive spectrometer (EDS) mapping was conducted, in which the Si and Ca signal was collected by EDS, and the C and N signals were collected by EDS maps. For the thermogravimetric analysis (TGA), the sample was placed in a ceramic crucible and heated from environment temperature to 800 °C within a TG analyzer (Nanjin Dazhan Institute of Electromechanical Technology STA-200, China). Fourier transform infrared spectroscopy (FTIR) analysis was performed on a Bruker Equinox 55 instrument to examine the chemical groups of BG-PDA. Approximately 20 mg of BG, BG-PDA or PDA particles were immersed in simulated body fluid (SBF, Na^+ 142 mmol/L, K^+ 5.0 mmol/L, Mg^{2+} 1.5 mmol/L, Ca^{2+} 2.5 mmol/L, Cl^- 147.8 mmol/L, HCO^{3-} 1.0 mmol/L, SO_4^{2-} 0.5 mmol/L, pH = 7.25) at 37 °C. After being immersed in SBF for 12 h or 7 days, the particles underwent a gentle washing with deionized water and were

air-dried in a vacuum oven. The mineralization ability of BG-PDA was investigated by X-ray diffraction (XRD, D/max-2500, Rigaku). Zeta potentials of coacervate microdroplets were measured on the Malvern Zetasizer (Nano ZS) instrument at room temperature.

2.3. THP-1 macrophages culture and conditioned medium collection

THP-1 cells were cultured in RPMI 1640 containing 10 % FBS, 1 % penicillin, and 1 % streptomycin at 37 °C in a humidified atmosphere with 5 % CO_2. THP-1 cells treated with PMA (100 ng/mL) for 6 h to obtain PMA-induced THP-1 macrophages. For M1 macrophage activation, THP-1 macrophages were cultured with medium containing 1 μg/mL LPS (*Escherichia coli*) and 20 ng/mL IFN-γ. M1 macrophages were cultured with medium containing 0.1 mg/mL BG-PDA or BG particles for another 24 h, referred to as BG-PDA or BG group and cultured with ordinary medium, referred to as M1 group. Supernatants of three groups were collected and centrifuged at 5000 rpm for 5 min as a condition medium for the next indirect co-culture experiment.

2.4. The polarization of macrophages by flow cytometry analysis

Briefly, 1×10^6 macrophages were suspended in serum-free RPMI 1640 medium, incubated with blocking buffer, stained with primary antibody (CD86 polyclonal anti-human, CD206 monoclonal anti-human) and secondary antibody (goat secondary antibody to rabbit IgG, Alexa flour@ 488, Goat anti-mouse Alexa flour@ 647). Flow cytometry was performed on a BD FACS Aria II and analyzed with Flow Jo Software 10.0.

2.5. The expression of inflammation-related mRNA by real-time PCR analysis

The methods for total RNA extraction, reverse transcription, and real-time PCR assay were conducted following the procedures outlined in the previous study [13]. The primer sequences used in this study are provided in Table 1. Glyceraldehyde-3-phosphate dehydrogenase (GAPDH) was employed as a reference gene for result normalization. mRNA expression of the target genes was normalized to GAPDH and analyzed using the $2^{-\Delta\Delta}$Cq method.

2.6. The secretion of IL-1β and TNF-α of macrophages by ELISA

THP-1 macrophages were cultured as mentioned before. Supernatants of three groups were collected and centrifuged at 5000 rpm for 5 min. ELISA analyzed the secretions of IL-1β and TNF-α following instructions provided by the manufacturer.

Table 1
Primer sequences.

Gene	Sequence (5′-3′)
CXCL9	Forward: TGCAAGGAACCCCAGTAGTGA
	Reverse: GGTGGATAGTCCCTTGGTTGG
CXCL10	Forward: GTGGCATTCAAGGAGTACCTC
	Reverse: TGATGGCCTTCGATTCTGGATT
DMP-1	Forward: AGGAAGTCTCGCATCTCAGAG
	Reverse: TGGAGTTGCTGTTTTCTGTAGAG
DSPP	Forward: ATATTGAGGGCTGGAATGGGGA
	Reverse: TTTGTGGCTCCAGCATTGTCA
IL-1β	Forward: ATGATGGCTTATTACAGTGGCAA
	Reverse: GTCGGAGATTCGTAGCTGGA
IL-6	Forward:CCACTCACCTCTTCAGAACG
	Reverse:CATCTTTGGAAGGTTCAGGTTG
IL-10	Forward:GACTTTAAGGGTTACCTGGGTTG
	Reverse:TCACATGCGCCTTGATGTCTG
iNOS	Forward: TTCAGTATCACAACCTCAGCAAG
	Reverse: TGGACCTGCAAGTTAAAATCCC
GAPDH	Forward:GAAGGTGAAGGTCGGAGTC
	Reverse:GAGATGGTGATGGGATTTC
TGF-β	Forward: GTAGCTCTGATGAGTGCAATGAC
	Reverse: CAGATATGGCAACTCCCAGTG

2.7. Intracellular ROS of macrophages

The intracellular levels of ROS in macrophages were assessed by DHE in accordance with the guidelines provided by the manufacturer. Initially, the cells were rinsed by a serum-free medium twice, followed by incubation in a complete medium supplemented with 5 μM DHE at 37 °C in the dark for 30 min. Subsequently, the cells were washed twice with serum-free medium and subsequently collected for intracellular ROS analysis by flow cytometry.

2.8. MMPs of macrophages by immunofluorescence

The MMPs values of macrophages were determined using a JC-1 MMPs Assay Kit in accordance with the manufacturer's instructions by immunofluorescence. The cells were rinsed three times with serum-free medium and then incubated with JC-1 staining working solution at 37 °C for 20 min. The cells were washed twice with JC-1 dilution buffer and immediately observed using a confocal laser microscope (BX51; Olympus Optical, Tokyo, Japan).

2.9. The mitochondrial respiratory of macrophages by mitochondrial OCRs

To investigate the mitochondrial respiratory activity of macrophages, oxygen consumption rates (OCRs) were measured using XF24 Seahorse. The cells were pre-treated in a CO_2-free incubator in Seahorse XF assay medium for 60 min. For OCR analysis, the basal OCRs were first determined. Next, 1.5 μM Oligo, 1 μM Carbonyl cyanide 4-(trifluoromethoxy) phenylhydrazone (FCCP), and 1 μM rotenone/antimycin (R/A) were sequentially injected during real-time measurements. The respiratory parameters were calculated as follows: maximal respiration = maximum rate measurement after FCCP injection − minimum rate measurement after R/A injection; and ATP production = final rate measurement prior to Oligo injection − minimum rate measurement after Oligo injection.

2.10. HDPCs culture

Human dental pulp cells (hDPCs) were obtained from healthy third molars from 18 to 25-year-old volunteers with the approval of the university ethical committee and the approval of the ethics committee (PKUSSRB-202053006) according to our previous study [11]. The obtained hDPCs were cultured in DMEM containing 10 % FBS, 1 % penicillin, and streptomycin at 37 °C with 5 % CO_2. HDPCs were passaged at a ratio of 1:3 upon reaching 80 % confluence. Cells between 4 and 6 passages were used for all experiments. 4–6 passages were used for the next experiment.

2.11. MTT assays of hDPCs

hDPCs were seeded into a 96-well plate and co-cultured with 0.1 mg/mL BG-PDA or BG particles. After 1, 3 and 7 days, fresh media containing 5 mg/mL MTT were added and incubated for 4 h at 37 °C. Finally, the blue-purple crystals at every bottom of the plate were dissolved using 150 μL DMSO and detected at 465 nm by a microplate reader. Data were expressed as the percentage (%).

2.12. Odontogenic differentiation and mineralization of hDPCs

1×10^4 hDPCs per well were seeded into a 12-well plate and directly co-cultured with 0.1 mg/mL BG-PDA or BG particles for 7 days. Real-time PCR evaluated the expression of odontogenic differentiation mRNA *dentin sialophosphoprotein* (*DSPP*) and *dentin matrix protein-1*

(*DMP-1*). The primer sequences used in this study are provided in Table 1.

1×10^4 hDPCs per well were seeded into a 12-well plate and directly co-cultured with 0.1 mg/mL BG-PDA or BG particles in a mineralization-inducing medium, odontogenic inducing medium (OM, DMEM supplemented with 50 mg/L ascorbic acid and 10 mM β-glycerophosphate, with 100 ng/mL dexamethasone) for 21 days. For the semi-quantification of calcium levels, alizarin red from mineralized nodules was dissolved in 10 % cetylpyridinium chloride and measured at 562 nm using a microtiter plate reader.

2.13. Indirect coculture of hDPCs and macrophages

1×10^4 hDPCs per well were seeded into a 12-well plate and the condition media of BG-PDA or BG-treated macrophages was used to culture hDPCs for 24 h, and the condition media of M1 macrophages were used as M1 hDPCs groups. The expression of inflammation-related mRNA (IL-1β, TNF-α, IL-6, IL-10 and TGF-β) was evaluated by real-time RT-PCR. Experiments were run on triplicates and repeated three times.

2.14. Direct pulp capping in rat pulpitis

Animal ethics approval was granted by the local ethics committee (PKUIRB-LA2022051). They also fulfilled ARRIVE guidelines. The pulpitis model of rat maxillary first molar was slightly modified by the previous study [13,20]. All samples were randomly assigned to the trial group. After anesthesia and oral disinfection, an ultrasonic tip (ED15) was applied to penetrate the dentin of the first molar. Once the pulp was exposed, a serial of K files was sequentially applied to enlarge the area of the exposed pulp. A wet small cotton with 10 mg/mL LPS was used to stimulate pulp inflammation for 4 h. The inflamed pulp was rinsed with saline. iROOT BP or BG-PDA or BG were used for direct pulp capping with crown sealing of self-adhesive resin served as iROOT BP group (n = 6), BG group (n = 7) and BG-PDA group (n = 7). The inflamed pulp was only sealed with self-adhesive resin and served as an LPS group (n = 7).

2.15. Miro-CT analysis of dentin repair

4 weeks after surgery, micro-CT imaging of maxillary rat molar was performed using a SkyScan 1272 microfocus X-ray system (SkyScan®, Kontich, Belgium) with software including NRecon reconstruction®, CTAn 1.8®, and CTvol. The basic parameters of the scanner were as follows: voltage 90 kV, current 160 μA and exposure time about 3 min in drying conditions. The visualization of the first molar was digitally reconstructed, showing a sagittal plane of newly formed hard tissue or exposed pulp area. The calibration curve was prepared from the mineral reference phantom (Ratoc System Engineering); the CT value was converted to the calcification degree (mg/cm^3) and the degree of tooth mineralization was measured. To calibrate the mineral density measurement, the mineral reference phantom was scanned prior to all experimental specimens.

2.16. Histological evaluation scoring of inflammatory response and semiquantitative analysis of IHC staining

3 days or 4 weeks after pulp capping, the animals were sacrificed and maxillary teeth and bone were fixed, decalcified, and cut into 4-μm-thick sections. Hematoxylin-eosin (HE) staining was used for the evaluation score of inflammatory infiltration. Immunohistochemistry with anti-CD86 antibody (1:200) and anti-CD206 antibody (1:1000) were performed in those samples 3 days after pulp capping to evaluate macrophage infiltration according to the manufacturer's instructions. For the semiquantitative analysis of immunohistochemistry (IHC) stain, positive areas were quantified from 6 randomly selected fields with a magnification of 200 × within the limits of ROI from each animal sample. The percentage of the positive area was calculated according to previous studies by Image J software [21].

2.17. Statistical analysis

All experimental data were expressed as the mean ± standard deviation. Statistical analysis of all data was executed by a one-way analysis of variance (ANOVA) and Tukey's *t*-test using SPSS 20.0 (International Business Machines Corporation (IBM, USA) with $p < 0.05$ as a significance level.

3. Results

3.1. Characterization of BG-PDA

SEM results revealed that the application of PDA as a coating on the surface of BG did not induce any significant changes in particle size or morphology (Fig. 1A–C, E, G). After being immersed in SBF for 12 h, flake hydroxyapatite crystals were observed to precipitate on both BG and BG-PDA surfaces (Fig. 1B–D, F, H), as confirmed by the presence of characteristic peaks of hydroxyapatite (25.9°, 31.7°, 40.2°) in the XRD spectrum (Fig. 1S). After being immersed in SBF for 7 days, the XRD spectrum revealed the presence of more obvious characteristic peaks of hydroxyapatite (28.4°, 48.3°, 50.2°, 54.1°) on both BG and BG-PDA (Fig. S5). EDS analysis revealed the presence of carbon, nitrogen, calcium, and silicon elements on the surface of BG-PDA (Fig. 1M – P), whereas only calcium and silicon were detected on the surface of BG (Fig. 1I-L). Thermogravimetric analysis (TGA) exhibited a weight loss in BG, PDA, and BG-PDA within the temperature range of 100–200 °C, which can be attributed to water evaporation (Fig. 1Q). Beyond 200 °C, weight loss corresponded to PDA degradation. The calculated PDA ratio in BG-PDA was determined to be 10 *wt*%. FTIR spectra indicated the presence of the formation of indole-related structure at 1621 cm^{-1} [7] in BG-PDA and PDA, as well as the stretching vibration of O–H, N–H, and NH_2 between 3200 cm^{-1} to 3500 cm^{-1} [7] in both BG-PDA and PDA (Fig. 1R). The peaks observed at 1100 and 802 cm^{-1} in Fig. 1R were attributed to the Si–O bond [19] in BG and BG-PDA. Furthermore, the surface potential of BG-PDA exhibited a higher negative charge compared to that of BG (Fig. 1T). These results confirmed the successful coating of PDA on the surface of BG, and further indicated that BG-PDA retained remarkable bioactivity.

3.2. M2 polarization of inflammatory macrophages

To investigate the effects of BG-PDA and BG on M2 polarization of inflammatory macrophages, M1 macrophages were directly co-cultured with 0.1 mg/mL BG or BG-PDA. The flow cytometry results indicated that BG-PDA had the ability to increase the protein expression radio of CD206 and CD86 in macrophages, in comparison to the BG and M1 groups (Fig. 2A and B). Additionally, BG-PDA significantly inhibited the pro-inflammatory mRNA expression of IL-1β, CXCL9, iNOS and CXCL10 (Fig. 2C–F). Conversely, the anti-inflammatory mRNA expressions of TGF-β and IL-10 were significantly elevated by BG-PDA (Fig. 2G and H). Furthermore, BG-PDA effectively inhibited the secretion of IL-1β and TNF-α (Fig. 2I and J), as well as cellular ROS in THP-1 macrophages (Fig. 2K and L). These results suggested that BG-PDA can promote the M2 polarization of inflammatory macrophages.

3.3. Mitochondrial functions in inflammatory macrophages

To further explore the internal mechanism of M2 polarization by BG-PDA in inflammatory macrophages, MMPs and OCRs were investigated. The results showed that macrophages co-cultured with BG-PDA maintained MMPs, whereas both M1 macrophages and those co-cultured with BG experienced a loss of MMPs, suggesting a potential association with cellular senescence (Fig. 3A). Additionally, macrophages co-cultured with BG-PDA exhibited higher OCR levels compared to the other

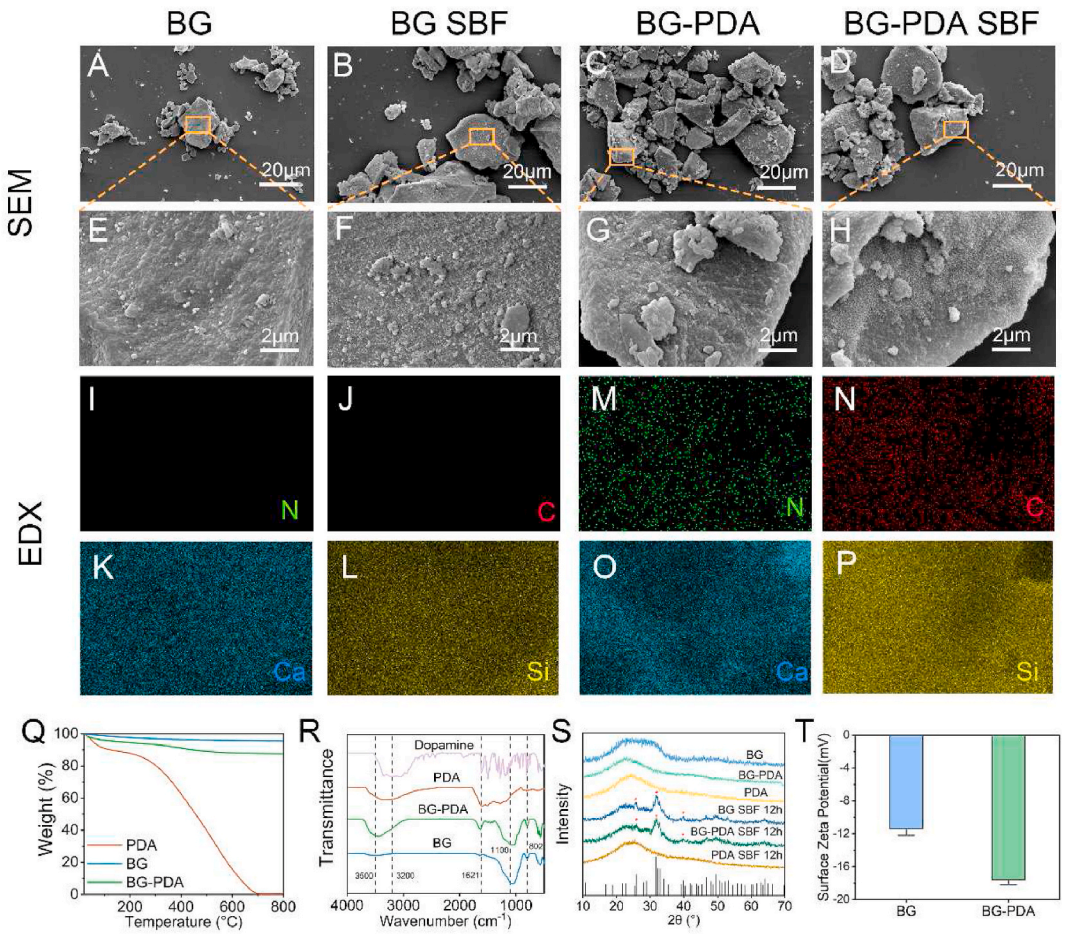

Fig. 1. Characteristics of BG-PDA. (A–H) SEM image of BG and BG-PDA before and after immersion in SBF for 12 h. (I–L) EDS results of BG. (M–P) EDS results of BG-PDA (Q) TGA result. (R) FITR results. (S) XRD results. (T) Zeta potential results.

groups, as depicted in Fig. 3B. Furthermore, the BG-PDA group demonstrated significant enhancements in basal respiration, maximal respiration, ATP production, and spare respiration, while no noticeable changes were observed in the BG group (Fig. 3C–F). These findings provide evidence that BG-PDA has the ability to enhance mitochondrial functions in inflammatory macrophages through the preservation of MMPs and the enhancement of mitochondrial respiration.

3.4. Odontogenesis promotion and inflammation inhibition by BG-PDA

To investigate the odontogenic effect of BG-PDA, hDPCs were co-cultured with 0.1 mg/mL BG or BG-PDA. MTT assay demonstrated that both BG-PDA and BG significantly enhanced the proliferation of hDPCs compared to the control group after 5 days (Fig. 4A). Live/dead staining showed that basically all cells were alive (labeled in green) and there were only a few scattered dead cells (labeled in red) after being co-cultured with 0.1 mg/mL BG or BG-PDA (Fig. S6). These results revealed that BG-PDA possess favorable biocompatibility. Furthermore, both BG-PDA and BG significantly upregulated the expression of odontogenesis-related mRNA (*DSPP* and *DMP-1*) in hDPCs, as determined by real-time PCR (Fig. 4B and C). Additionally, BG-PDA exhibited a superior mineralization-inducing capabilities in hDPCs compared to the BG group (Fig. 4D and E). Moreover, our study elucidated the impact of indirect co-culturing of hDPCs with BG or BG-PDA treated inflammatory macrophages (Fig. 4F–J). Both BG-PDA and BG demonstrated a significant inhibitory effect on the expression of pro-inflammatory mRNA (*IL-1β*, *IL-6*, and *TNF-α*), while simultaneously promoting the expression of *IL-10* and *TGF-β*, compared with hDPCs indirectly co-cultured with M1 macrophages. Notably, BG-PDA exhibited the most prominent effects in inhibiting the expression of *IL-1β* and *IL-6* and promoting the expression of *IL-10* among the three groups. These results suggested BG-PDA possessed the superior ability to promote odontogenic differentiation of hDPCs, and inhibit inflammation compared to BG.

3.5. Immunoregulatory effects of BG-PDA in rat pulpitis

To further elucidate the anti-inflammatory and immunoregulatory effects of BG-PDA *in vivo*, a pulpitis model was established in the maxillary first molar through a 4-h LPS stimulation. BG-PDA or BG particles were employed for direct pulp capping, with iROOT BP serving as the positive control. After three days of pulp capping, the LPS group exhibited a moderate level of inflammation in a portion of the coronal pulp (Fig. 5A, Fig. S7A). Similarly, the BG or iROOT BP groups exhibited mild to moderate levels of inflammation in a certain area of the coronal pulp adjacent to the exposed pulp area (Fig. 5B–C, Figs. S7B–C). In contrast, minimal inflammatory cell infiltration was observed in close proximity to the exposed pulp area, while the odontoblast cell layer remained predominantly intact in the BG-PDA group (Fig. 5D, Fig. S7D). A significant difference in the intensity score of inflammation was observed between the BG-PDA and LPS groups (Fig. 5E). Immunohistochemical (IHC) staining revealed distinct populations of macrophages across all four groups, characterized by the presence of $CD86^{-}$positive M1 macrophages and $CD206^{-}$positive M2 macrophages. The LPS group showed a significant upregulation of CD86-positive M1 macrophages (Fig. 5F) and a downregulation of CD206-positive M2 macrophages (Fig. 5K). Conversely, the BG-PDA group exhibited a pronounced a

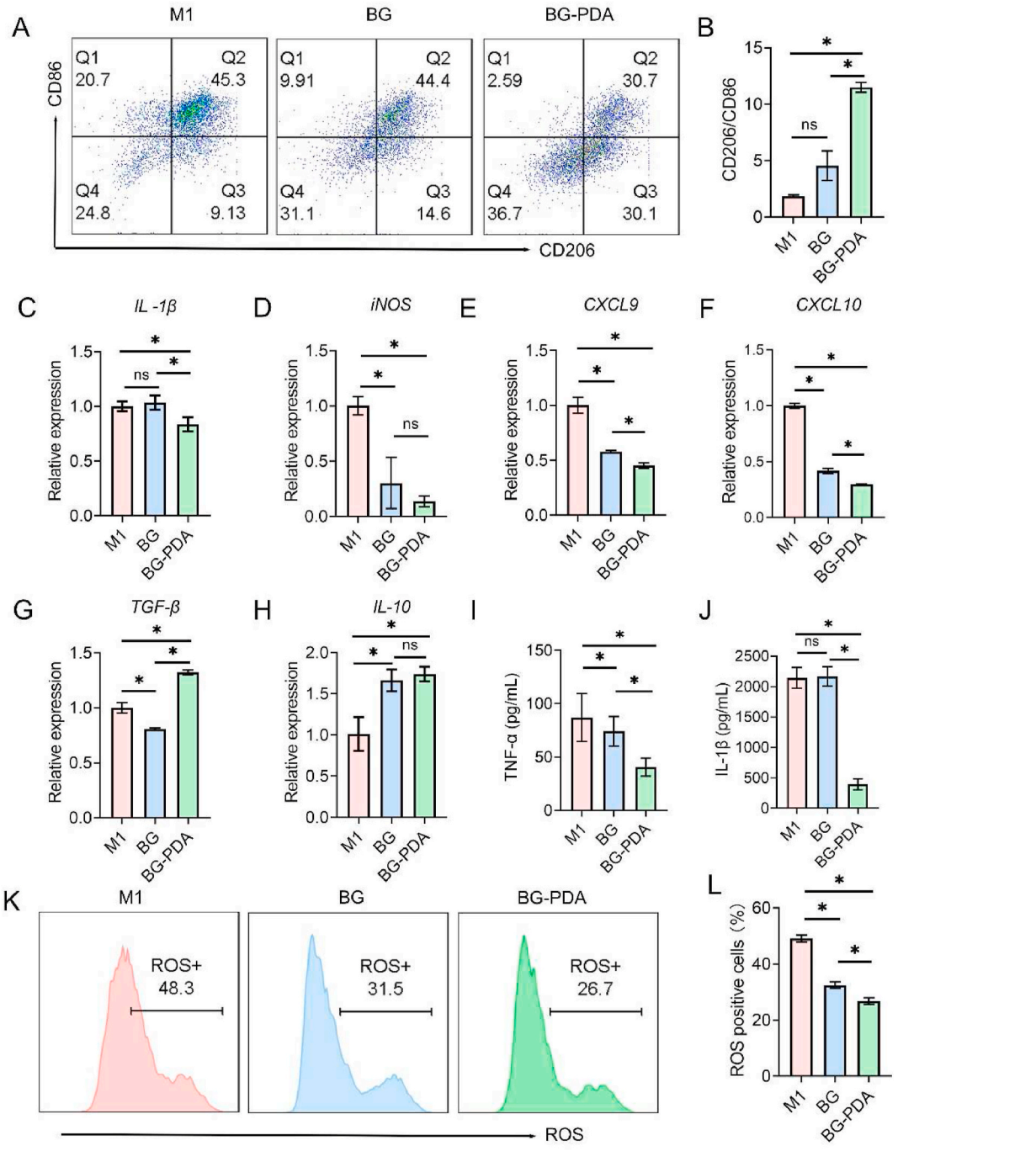

Fig. 2. M2 polarization of inflammatory macrophages by BG-PDA. (A) The expression of CD86 and CD206 in macrophages by flow cytometry. (B) Quantitative analysis of CD206/CD86 positive macrophages; (C–H) The mRNA expression of inflammation-related mRNA (*IL-1β*, *iNOS*, *CXCL9*, *CXCL10*, *IL-10* and *TGF-β*) in macrophages by Real-Time PCR; (I–J) The secretion of IL-1β and TNF-α by ELISA. (K) Intracellular ROS by flow cytometry. (L) Quantitative analysis of ROS-positive macrophages. Data were presented as means ± SD. "*" $P < 0.05$.

downregulation of CD86-positive M1 macrophages (Fig. 5I) and upregulation of CD206-positive M2 macrophages (Fig. 5N). The $CD86^{-}$positive M1 macrophages exhibited a significantly smaller area in the BG-PDA group compared to the LPS group (Fig. 5J), while the $CD206^{-}$positive M2 macrophages displayed a significantly larger area in the BG-PDA group compared to the other groups (Fig. 5O). These results provide evidence supporting the anti-inflammatory and immunoregulatory properties of BG-PDA in the context of rat pulpitis.

3.6. Dentin repair promoted by BG-PDA in rat pulpitis

To further investigate the *in vivo* dentin repair ability, BG-PDA or BG particles were utilized as pulp capping materials to treat pulpitis in the maxillary first molar of rats, with iROOT BP serving as a positive control. After 4 weeks, the extent of dentin repair adjacent to the exposed pulp region was assessed using micro-CT and HE staining. Notably, in the LPS group, a discernible absence of dentin repair surrounding the exposed pulp region was observed (Fig. 5P and U, Fig. S7E). Conversely, the iROOT BP, BG-PDA, and BG groups exhibited varying levels of dentin repair in the vicinity of the exposed pulp region (Fig. 5Q–S, Fig. 5V–X,

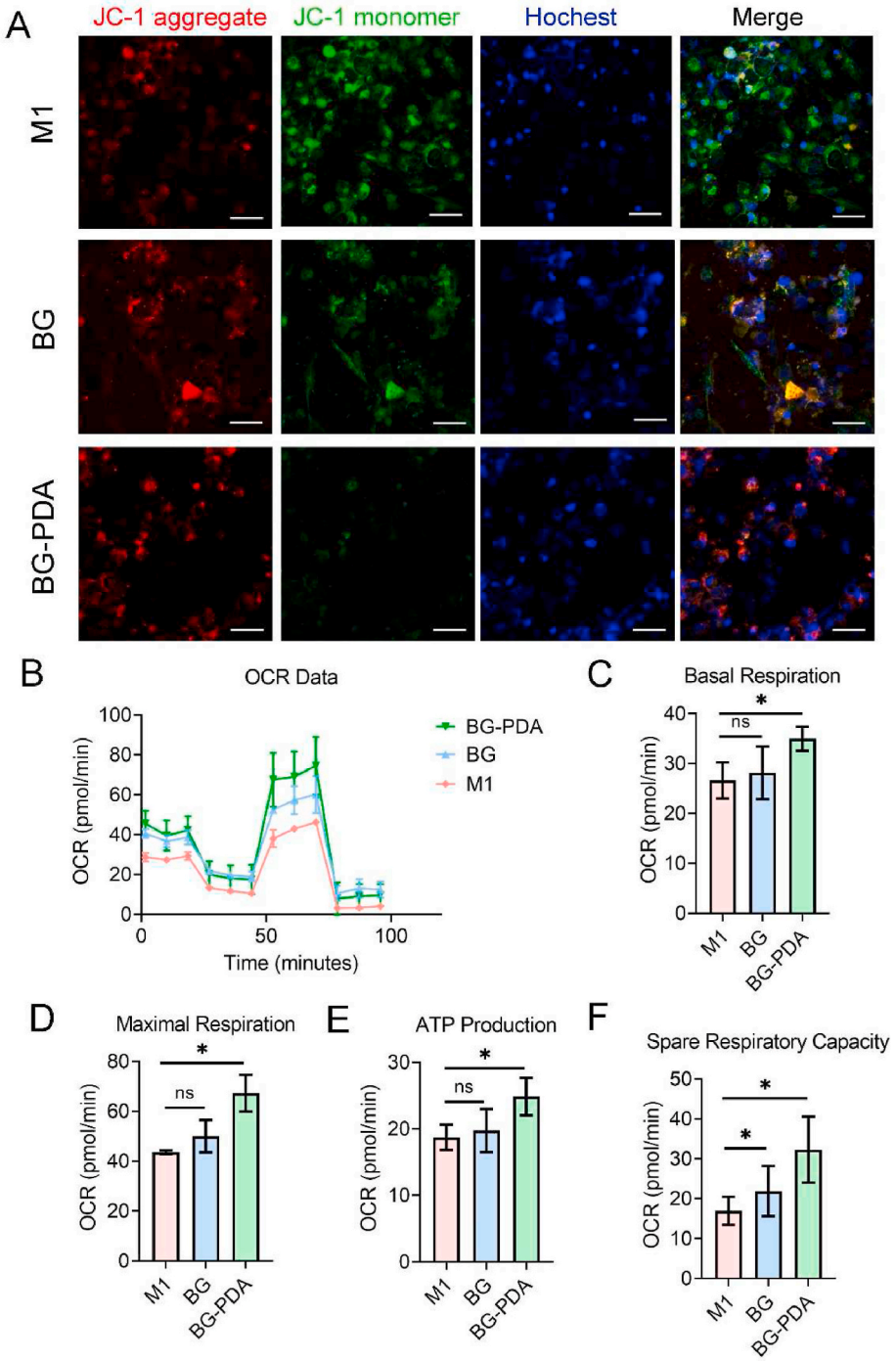

Fig. 3. Mitochondrial functions in inflammatory macrophages regulated by BG-PDA. (A) MMPs of macrophages by JC-1 immunofluorescent staining. Red, JC-1 aggregation in healthy mitochondria; green, cytosolic JC-1 monomers in mitochondria with MMPs lost; blue, cell nuclear. (B) Real-time OCR of macrophages in response to sequential treatment with Oligo, FCCP, and rotenone by cell mitochondrial stress test. (C–F) Quantitative analysis of basal respiration, maximal respiration, ATP production and spare respiratory capacity (n = 3). Data were presented as means ± SD. Scale bar: 20 μm; "*", $P < 0.05$. (For interpretation of the references to color in this figure legend, the reader is referred to the Web version of this article.)

Figs. S7F–H). Notably, the BG-PDA group demonstrated a significantly higher volume of dentin surrounding the exposed pulp region compared to the iROOT BP group, while no significant difference was observed between the iROOT BP and BG groups (Fig. 5T). Furthermore, there was no significant difference in dentin density among all three groups (Fig. 5Y). These results verified that BG-PDA possess the potential to enhance dentin repair in cases of rat pulpitis.

4. Discussion

Inflammation plays a pivotal role in healing processes, with macrophages emerging as key regulators capable of either facilitating tissue repair or inducing damage, depending on their response to the surrounding microenvironment. Therefore, the utilization of biomaterials that possess the capacity to effectively regulate the host immune system, thereby promoting the repair of inflamed pulp tissue, holds significant promise in clinical application [22]. In this study, we successfully

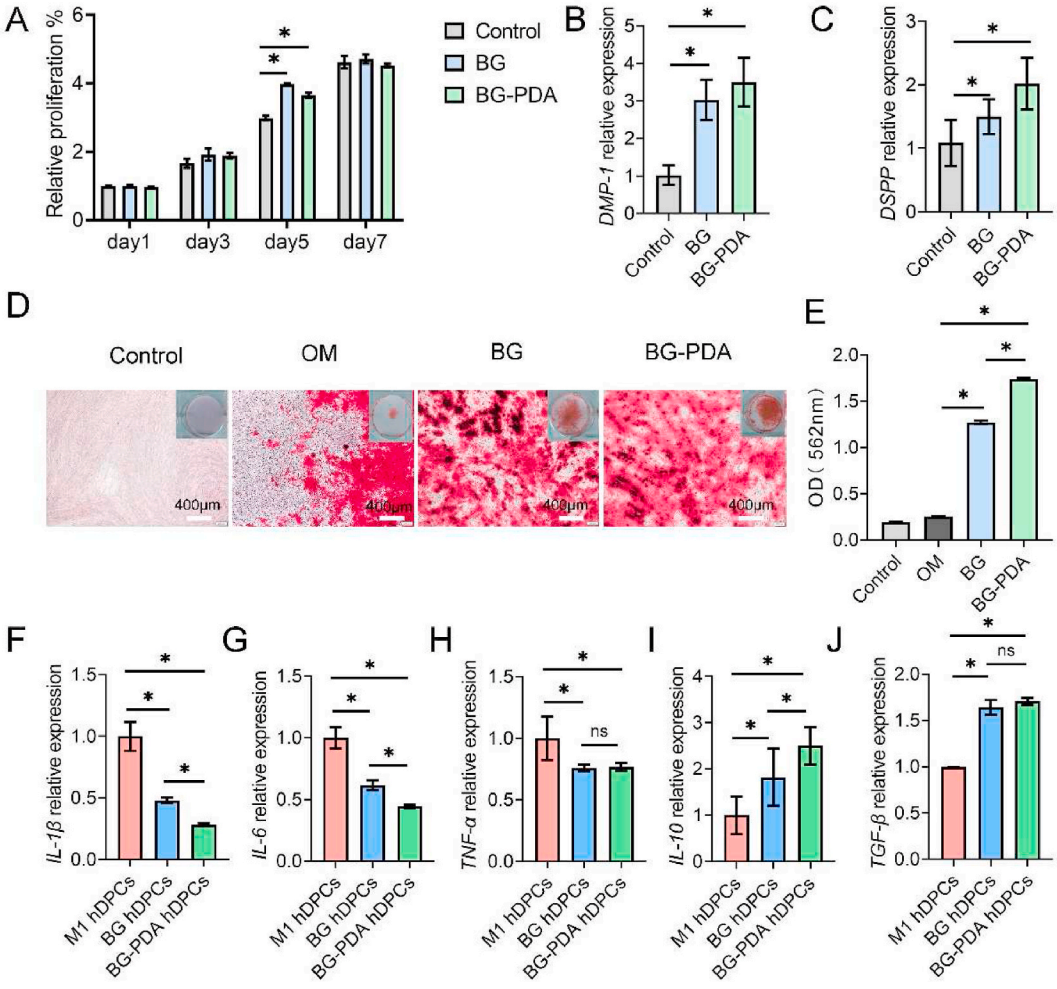

Fig. 4. Odontogenic differentiation promotion and inflammation inhibition by BG-PDA. (A) MTT results; (B–C) DMP-1 and DSPP expression by Real-Time PCR. (D–E) Mineralization by alizarin red. (F–J) The expression of inflammation-related mRNA (*IL-1β*, *TNF-α*, *IL-10*, *TGF-β*) by Real-Time PCR in hDPCs. Data were presented as means ± SD. "*", $P < 0.05$. (For interpretation of the references to color in this figure legend, the reader is referred to the Web version of this article.)

developed BG-PDA as a ROS scavenger and immune-regulated biomaterial, specifically designed for the purpose of repairing inflamed pulp. This study investigated the biological effects of BG-PDA, specifically its influence on phenotypic transformation, intracellular ROS levels, and mitochondrial function in macrophages, as well as its odontogenic effects in hDPCs. In a rat model of pulpitis, BG-PDA demonstrated remarkable anti-inflammatory properties, immune regulation, and the ability to facilitate dentin repair. The results showed that BG-PDA could accelerate the healing process of inflamed pulp by promoting M2 macrophage polarization and enhancing mitochondrial function.

Previous research has elucidated the pivotal role of M2 macrophage polarization in alleviating inflammation and facilitating tissue regeneration [23]. The present study aimed to investigate the potential impact of the interaction between macrophages and dental pulp cells. Consistently with expectations, BG-PDA was observed to promote polarization of M2 macrophages within the inflammatory microenvironment. The regulation ability of BG-PDA may be related to the ROS scavenging ability of the PDA coating, the surface potential and morphology changes, and the change of BG ion release rate of the inner layer. Calcium and ROS play a pivotal role as critical signaling molecules in regulating various cellular functions. Our study confirmed that the ion release concentration of BG-PDA is slower than that of BG (Fig. S1). The surface potential decreases and becomes more negative after PDA modification, which would affect the release of cations. The immune-regulatory and tissue repair effects of BG and BG-PDA were related to the release of calcium and silicon ions, with the magnitude of these effects being dependent on the concentration [24]. It has been shown that the sustained release of calcium ions promotes the regulation of M2 macrophage polarization and facilitates bone tissue repair [25]. Additionally, the neutralization of ROS by PDA improved the inflammatory microenvironment and promotes M2 polarization. It is noteworthy that macrophages can influence stem cells through paracrine effects [26]. Our findings highlighted the anti-inflammatory properties of BG-PDA when indirectly co-cultured with hDPCs and macrophages. Furthermore, BG-PDA demonstrated a superior ability to promote odontogenic differentiation in hDPCs compared to BG alone. Previous study extensively demonstrated the capacity of BG to induce odontogenesis in healthy dental pulp cells [13]. Our study is consistent with previous research on PDA-coated mineral trioxide aggregate (MTA), which has been shown to promote odontogenic differentiation of dental pulp cells *in vitro* [18].

The application of BG-PDA has been found to possess both immunoregulatory and odontogenesis-inducing effects on inflamed pulp, eventually promoting enhanced dentin repair *in vivo*. Chung et al. observed persistent pulp inflammation in the majority of rat teeth despite being treatment with calcium silicate cements [27]. It is suggested that using calcium silicate cements as pulp capping materials may be less effective in cases of inflamed pulp compared to healthy pulp. However, our study demonstrated that applying BG-PDA effectively stimulates the polarization of M2 macrophages within the inflamed pulp

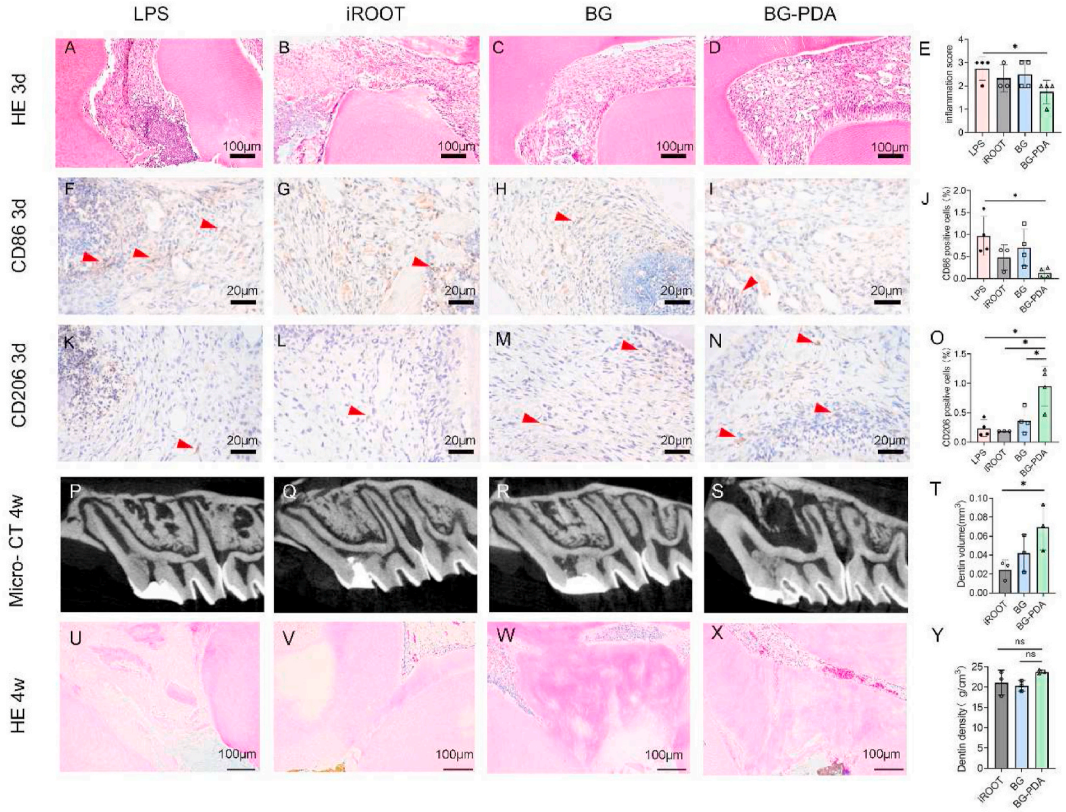

Fig. 5. Anti-inflammatory, immunoregulatory and dentin repair effects of BG-PDA in rat pulpitis. 3 days after direct pulp capping, the inflammatory response of dental pulp in rat first molar determined by (A–D) HE staining. (F–I) $CD86^+$ M1 macrophages determined by IHC staining. (K–N) $CD206^+$ M2 macrophages determined by IHC staining. (E) The semiquantitative analysis of inflammatory response score. (J&O) The semiquantitative analysis of CD86 and CD206 positive cells. (n = 3 in iROOT group, n = 4 in the other three groups). 4 weeks after direct pulp capping, the dentin repair of dental pulp in rat first molar determined by (P–S) Vertical plane images of Micro CT and (U–X) vertical tissue slices of HE staining. (T&Y) Quantitative analysis of dentin volume and mineral density (n = 3). Data were presented as means ± SD with scatter. "*", $P < 0.05$.

tissue, which is consistent with the findings of *in vitro* experiments. The above findings verified the ability of BG-PDA for immune regulation and odontogenic differentiation.

The polarization phenotypes of macrophages are significantly influenced by mitochondrial metabolism [28]. The transition between glycolysis and mitochondrial oxidative phosphorylation has been associated with macrophage polarization. Within the inflammatory microenvironment, the presence of LPS triggers various mitochondrial alteration, including fission, fragmentation, MMP depolarization, and a transition from ATP synthesis to ROS production. These changes ultimately facilitate the generation of pro-inflammatory factors through the activation of the NF-κB pathway [29]. The excessive generation of ROS hinders tissue repair by elevating oxidative stress and inducing DNA damage. PDA possesses multiple phenol groups, which can donate protons or electrons to stabilize free radicals, including extracellular ROS [30]. In this study, it has been observed that BG-PDA effectively decreased intracellular ROS levels, as determined by flow cytometry analysis. Remarkably, the results revealed that BG-PDA protected MMPs against depolarization caused by harmful ROS and enhanced oxidative phosphorylation efficiency *in vitro*. The present findings offered valuable insights into the immune regulation mechanism facilitated by BG-PDA. Additionally, Willenborg et al. demonstrated that mitochondrial respiration serves as a distinguishing feature of pro-resolving wound macrophages during rat skin wounds healing process. This observation emphasized the insufficiency of relying solely on glycolytic metabolism for efficient repair during the initial phase [31].

An increasing body of evidence has substantiated the exceptional anti-oxidation and anti-inflammatory ability of PDA composite biomaterial [32,33]. Drawing inspiration from the adhesive properties of mussels, the acquisition of a PDA coating through spontaneous oxidation and self-polymerization has been demonstrated as a straightforward procedure [34]. The BG particles used in present study is composed by varying sizes under 74 μm, which may contain a part of nano particles. To demonstrate that the PDA are coated on the surface and not just mixed with BG, we utilized differential centrifugation to obtain pure BG-PDA components and PDA nanoparticles resulting from dopamine self-polymerization were excluded as far as possible. We used 5000 rpm to centrifuge BG-PDA during the synthesizing process. In contrast, PDA nanoparticles require more than 10000 rpm to be centrifuged into a precipitate. Thus, most of the spontaneous formatted PDA nanoparticles still exist in the supernatant and have been thrown away during the synthesizing process of BG-PDA. SEM results of BG-PDA revealed that there are no spherical structures similar to PDA nanoparticles was observed (Fig. 1C, . G, and Fig. S4). Combined with TEM, TGA, FTIR and Zeta potential results, we can conclude that PDA the principal component of prepared material is PDA coated BG particles in the micron scale. This aforementioned evidence establishes a solid foundation for the potential application of PDA-coated material in the context of dental pulp inflammation. By manipulating the mass ratio and reaction time, it is feasible to attain a stable proportional coating of PDA on BG [35]. This study demonstrates that BG-PDA maintains favorable mineralization activity *in vitro*. Liu et al. discovered that PDA enhances the mineralization capacity of calcium phosphate cement by promoting the conversion of dicalcium phosphate dihydrate and α-tricalcium phosphate to hydroxyapatite (HA) during the initial stages [36]. The hydroxyl and amine groups within PDA offer potential nucleation sites for calcium phosphate [37].

Our study has successfully confirmed the efficiency of BG-PDA in

modulating macrophage activity and promoting dentin repair in inflamed dental pulp, thereby presenting a promising clinical prospect for the management of dental pulp inflammation. However, it is imperative to acknowledge the limitations inherent in our study. Additional investigation is necessary to elucidate the principal signaling pathways of BG-PDA involved in macrophage mitochondria, in order to obtain a more comprehensive comprehension of the underlying molecular mechanisms. Concurrently, we have successfully constructed a moderate inflammation model of dental pulp in the maxillary first molar of rats. In future investigations, we intend to explore the impact of BG-PDA on a severe inflammation model and modify the material to enhance its antibacterial ability, thereby augmenting our understanding in this domain.

5. Conclusion

We have successfully synthesized a PDA-coated BG (BG-PDA) and investigated its performance in immunoregulation and odontogenesis for VPT. Our findings demonstrate that BG-PDA facilitates M2 polarization, inhibits intracellular ROS levels, by enhancing mitochondrial functionality through the preservation of MMPs and the augmentation of oxidative phosphorylation. Moreover, BG-PDA promotes odontogenic differentiation of hDPCs, exhibits remarkable anti-inflammatory properties, and stimulates the formation of restorative dentin in a rat model of pulpitis. This study provides a potentially novel insight into vital pulp therapy for pulpitis.

CRediT authorship contribution statement

Jingyi Li: Writing – review & editing, Writing – original draft, Visualization, Validation, Software, Methodology, Investigation, Formal analysis, Data curation, Conceptualization. **Jilin Wu:** Writing – review & editing, Writing – original draft, Visualization, Validation, Supervision, Methodology, Investigation, Formal analysis, Data curation, Conceptualization. **Lin Zhu:** Supervision, Software, Methodology, Investigation, Data curation. **Sicong Mao:** Software, Methodology, Investigation, Formal analysis, Data curation. **Sainan Wang:** Visualization, Validation, Supervision, Resources, Project administration, Methodology, Conceptualization. **Peipei Jia:** Supervision, Software, Methodology, Investigation, Data curation. **Yanmei Dong:** Writing – review & editing, Writing – original draft, Supervision, Software, Resources, Project administration, Funding acquisition, Formal analysis, Conceptualization.

Declaration of competing interest

The authors declare that they have no known competing financial interests or personal relationships that could have appeared to influence the work reported in this paper.

Data availability

Data will be made available on request.

Acknowledgements

The authors are grateful for the support of the National Natural Science Foundation of China (81870753 and 82370946), Peking University Medicine Sailing Program for Young Scholars' Scientific & Technological Innovation and the Fundamental Research Funds for the Central Universities (BMU2024YFJHPY038). We also thank Prof. Dong Qiu (Institute of Chemistry, Chinese Academy of Sciences, Beijing, China) for generously offering the BG materials.

Appendix A. Supplementary data

Supplementary data to this article can be found online at https://doi.org/10.1016/j.mtbio.2024.101130.

References

[1] S.G. Kim, M. Malek, A. Sigurdsson, L.M. Lin, B. Kahler, Regenerative endodontics: a comprehensive review, Int. Endod. J. 51 (12) (2018) 1367–1388, https://doi.org/10.1111/iej.12954.
[2] A. Covarrubias, V. Byles, T. Horng, ROS sets the stage for macrophage differentiation, Cell Res. 23 (8) (2013) 984–985, https://doi.org/10.1038/cr.2013.88.
[3] M. Zhao, Y. Wang, L. Li, S. Liu, C. Wang, Y. Yuan, G. Yang, Y. Chen, J. Cheng, Y. Lu, J. Liu, Mitochondrial ROS promote mitochondrial dysfunction and inflammation in ischemic acute kidney injury by disrupting TFAM-mediated mtDNA maintenance, Theranostics 11 (4) (2021) 1845–1863, https://doi.org/10.7150/thno.50905.
[4] M.M. Mehta, S.E. Weinberg, N.S. Chandel, Mitochondrial control of immunity: beyond ATP, Nat. Rev. Immunol. 17 (10) (2017) 608–620, https://doi.org/10.1038/nri.2017.66.
[5] R. Stienstra, R.T. Netea-Maier, N.P. Riksen, L. Joosten, M.G. Netea, Specific and complex reprogramming of cellular metabolism in myeloid cells during innate immune responses, Cell Metabol. 26 (1) (2017) 142–156, https://doi.org/10.1016/j.cmet.2017.06.001.
[6] J. Hu, L. Yang, P. Yang, S. Jiang, X. Liu, Y. Li, Polydopamine free radical scavengers, Biomater. Sci. 8 (18) (2020) 4940–4950, https://doi.org/10.1039/d0bm01070g.
[7] X. Bao, J. Zhao, J. Sun, M. Hu, X. Yang, Polydopamine nanoparticles as efficient scavengers for reactive oxygen species in periodontal disease, ACS Nano 12 (9) (2018) 8882–8892, https://doi.org/10.1021/acsnano.8b04022.
[8] W. Ma, X. Zhang, Y. Liu, L. Fan, J. Gan, W. Liu, Y. Zhao, L. Sun, Polydopamine decorated microneedles with Fe-MSC-Derived nanovesicles encapsulation for wound healing, Adv. Sci. 9 (13) (2022), https://doi.org/10.1002/advs.202103317.
[9] L. Jin, F. Yuan, C. Chen, J. Wu, R. Gong, G. Yuan, H. Zeng, J. Pei, T. Chen, Degradation products of polydopamine restrained inflammatory response of LPS-stimulated macrophages through mediation TLR-4-MYD88 dependent signaling pathways by antioxidant, Inflammation 42 (2) (2019) 658–671, https://doi.org/10.1007/s10753-018-0923-3.
[10] O. Demir-Oguz, A.R. Boccaccini, D. Loca, Injectable bone cements: what benefits the combination of calcium phosphates and bioactive glasses could bring? Bioact. Mater. 19 (2023) 217–236, https://doi.org/10.1016/j.bioactmat.2022.04.007.
[11] C. Cui, S. Wang, H. Ren, A. Li, D. Qiu, Y. Gan, Y. Dong, Regeneration of dental-pulp complex-like tissue using phytic acid derived bioactive glasses, RSC Adv. 7 (36) (2017) 22063–22070, https://doi.org/10.1039/c7ra01480e.
[12] Y. Long, S. Liu, L. Zhu, Q. Liang, X. Chen, Y. Dong, Evaluation of pulp response to novel bioactive glass pulp capping materials, J. Endod. 43 (10) (2017) 1647–1650.
[13] J. Li, S. Wang, Y. Dong, Regeneration of pulp-dentine complex-like tissue in a rat experimental model under an inflammatory microenvironment using high phosphorous-containing bioactive glasses, Int. Endod. J. 54 (7) (2021) 1129–1141, https://doi.org/10.1111/iej.13505.
[14] K. Zheng, W. Niu, B. Lei, A.R. Boccaccini, Immunomodulatory bioactive glasses for tissue regeneration, Acta Biomater. 133 (2021) 168–186, https://doi.org/10.1016/j.actbio.2021.08.023.
[15] Z. Li, K. Xie, S. Yang, T. Yu, Y. Xiao, Y. Zhou, Multifunctional Ca-Zn-Si-based micro-nano spheres with anti-infective, anti-inflammatory, and dentin regenerative properties for pulp capping application, J. Mater. Chem. B 9 (39) (2021) 8289–8299, https://doi.org/10.1039/d1tb01517f.
[16] M.L. Alfieri, T. Weil, D. Ng, V. Ball, Polydopamine at biological interfaces, Adv. Colloid Interface Sci. 305 (2022) 102689, https://doi.org/10.1016/j.cis.2022.102689.
[17] Z. Deng, W. Wang, X. Xu, Y. Nie, Y. Liu, O. Gould, N. Ma, A. Lendlein, Biofunction of polydopamine coating in stem cell culture, ACS Appl. Mater. Interfaces 13 (9) (2021) 10748–10759, https://doi.org/10.1021/acsami.0c22565.
[18] M.G. Tu, C.C. Ho, T.T. Hsu, T.H. Huang, M.J. Lin, M.Y. Shie, Mineral trioxide aggregate with mussel-inspired surface nanolayers for stimulating odontogenic differentiation of dental pulp cells, J. Endod. 44 (6) (2018) 963–970, https://doi.org/10.1016/j.joen.2018.02.018.
[19] A. Li, Y. Lv, H. Ren, Y. Cui, C. Wang, R.A. Martin, D. Qiu, In vitro evaluation of a novel pH neutral calcium phosphosilicate bioactive glass that does not require preconditioning prior to use, Int. J. Appl. Glass Sci. 8 (4) (2017) 403–411, https://doi.org/10.1111/ijag.12321.
[20] E. Renard, A. Gaudin, G. Bienvenu, J. Amiaud, J.C. Farges, M.C. Cuturi, A. Moreau, B. Alliot-Licht, Immune cells and molecular networks in experimentally induced pulpitis, J. Dent. Res. 95 (2) (2016) 196–205, https://doi.org/10.1177/0022034515612086.
[21] H. Xu, Y. Zhu, A.W. Hsiao, J. Xu, W. Tong, L. Chang, X. Zhang, Y.F. Chen, J. Li, W. Chen, Y. Zhang, H.F. Chan, C.W. Lee, Bioactive glass-elicited stem cell-derived extracellular vesicles regulate M2 macrophage polarization and angiogenesis to improve tendon regeneration and functional recovery, Biomaterials 294 (2023) 121998, https://doi.org/10.1016/j.biomaterials.2023.121998.
[22] R. Dal-Fabbro, W.B. Swanson, L.C. Capalbo, H. Sasaki, M.C. Bottino, Next-generation biomaterials for dental pulp tissue immunomodulation, Dent. Mater. 39 (4) (2023) 333–349, https://doi.org/10.1016/j.dental.2023.03.013.

[23] T.A. Wynn, K.M. Vannella, Macrophages in tissue repair, regeneration, and fibrosis, Immunity 44 (3) (2016) 450–462, https://doi.org/10.1016/j.immuni.2016.02.015.
[24] W. Xie, X. Fu, F. Tang, Y. Mo, J. Cheng, H. Wang, X. Chen, Dose-dependent modulation effects of bioactive glass particles on macrophages and diabetic wound healing, J. Mater. Chem. B 7 (6) (2019) 940–952, https://doi.org/10.1039/c8tb02938e.
[25] J. Zhang, Q. Wu, C. Yin, X. Jia, Z. Zhao, X. Zhang, G. Yuan, H. Hu, Q. Zhao, Sustained calcium ion release from bioceramics promotes CaSR-mediated M2 macrophage polarization for osteoinduction, J. Leukoc. Biol. 110 (3) (2021) 485–496, https://doi.org/10.1002/JLB.3MA0321-739R.
[26] J. Pajarinen, T. Lin, E. Gibon, Y. Kohno, M. Maruyama, K. Nathan, L. Lu, Z. Yao, S. B. Goodman, Mesenchymal stem cell-macrophage crosstalk and bone healing, Biomaterials 196 (2019) 80–89, https://doi.org/10.1016/j.biomaterials.2017.12.025.
[27] M. Chung, S. Lee, S. Kim, E. Kim, Inflammatory response and odontogenic differentiation of inflamed dental pulp treated with different pulp capping materials: an in vivo study, Int. Endod. J. 56 (9) (2023) 1118–1128, https://doi.org/10.1111/iej.13947.
[28] E.L. Mills, B. Kelly, A. Logan, A. Costa, M. Varma, C.E. Bryant, P. Tourlomousis, J. Dabritz, E. Gottlieb, I. Latorre, S.C. Corr, G. McManus, D. Ryan, H.T. Jacobs, M. Szibor, R.J. Xavier, T. Braun, C. Frezza, M.P. Murphy, L.A. O'Neill, Succinate dehydrogenase supports metabolic repurposing of mitochondria to drive inflammatory macrophages, Cell 167 (2) (2016) 457–470.e13, https://doi.org/10.1016/j.cell.2016.08.064.
[29] R.P. Chakrabarty, N.S. Chandel, Mitochondria as signaling organelles control mammalian stem cell fate, Cell Stem Cell 28 (3) (2021) 394–408, https://doi.org/10.1016/j.stem.2021.02.011.
[30] Q. Dai, H. Geng, Q. Yu, J. Hao, J. Cui, Polyphenol-based particles for theranostics, Theranostics 9 (11) (2019) 3170–3190, https://doi.org/10.7150/thno.31847.
[31] S. Willenborg, D.E. Sanin, A. Jais, X. Ding, T. Ulas, J. Nuchel, M. Popovic, T. MacVicar, T. Langer, J.L. Schultze, A. Gerbaulet, A. Roers, E.J. Pearce, J. C. Bruning, A. Trifunovic, S.A. Eming, Mitochondrial metabolism coordinates stage-specific repair processes in macrophages during wound healing, Cell Metabol. 33 (12) (2021) 2398–2414.e9, https://doi.org/10.1016/j.cmet.2021.10.004.
[32] M. Bao, K. Wang, J. Li, Y. Li, H. Zhu, M. Lu, Y. Zhang, Q. Fan, L. Han, K. Wang, D. Wang, Y. Gao, B. Peng, Z. Ming, W. Liu, ROS Scavenging and inflammation-directed polydopamine nanoparticles regulate gut immunity and flora therapy in inflammatory bowel disease, Acta Biomater. 161 (2023) 250–264, https://doi.org/10.1016/j.actbio.2023.02.026.
[33] X. Lou, Y. Hu, H. Zhang, J. Liu, Y. Zhao, Polydopamine nanoparticles attenuate retina ganglion cell degeneration and restore visual function after optic nerve injury, J. Nanobiotechnol. 19 (1) (2021) 436, https://doi.org/10.1186/s12951-021-01199-3.
[34] H. Lee, S.M. Dellatore, W.M. Miller, P.B. Messersmith, Mussel-inspired surface chemistry for multifunctional coatings, Science 318 (5849) (2007) 426–430, https://doi.org/10.1126/science.1147241.
[35] V. Ball, Polydopamine nanomaterials: recent advances in synthesis methods and applications, Front. Bioeng. Biotechnol. 6 (2018) 109, https://doi.org/10.3389/fbioe.2018.00109.
[36] Z. Liu, S. Qu, X. Zheng, X. Xiong, R. Fu, K. Tang, Z. Zhong, J. Weng, Effect of polydopamine on the biomimetic mineralization of mussel-inspired calcium phosphate cement in vitro, Mater. Sci. Eng., C 44 (2014) 44–51, https://doi.org/10.1016/j.msec.2014.07.063.
[37] U. Amornkitbamrung, Y. In, Z. Wang, J. Song, S.H. Oh, M.H. Hong, H. Shin, c-Axis-Oriented platelets of crystalline hydroxyapatite in biomimetic intrafibrillar mineralization of polydopamine-functionalized collagen type I, ACS Omega 7 (6) (2022) 4821–4831, https://doi.org/10.1021/acsomega.1c05198.